Self-Biased Boron-10 Coated High-Purity Epitaxial GaAs Thermal Neutron Detectors

D.S. McGregor[1], S.M. Vernon[2], H.K. Gersch[1], S.M. Markham[2], S.J. Wojtczuk[2] and D.K. Wehe[1]
[1]Department of Nuclear Engineering and Radiological Sciences, University of Michigan, Ann Arbor, MI 48109-2104
[2]Spire Corporation, 1 Patriots Park, Bedford, MA 01730-2396

Abstract

Semiconductor thermal neutron detection devices based on ^{10}B-coated high-purity GaAs films were investigated. The fundamental device consisted of high-purity ν-type epitaxial GaAs films grown onto n-type GaAs substrates. Two blocking contact adaptations were applied to the high-purity ν-type GaAs regions: 2000 Å thick p+ GaAs blocking contacts and 200 Å thick Schottky blocking contacts.

The ν-type GaAs active layers ranged between 1 micron and 5 microns in thickness. The device sensitive areas were 3mm x 3mm, each of which was coated with a 1.5mm diameter film of 98% enriched high-purity ^{10}B. The built-in potential of the blocking contact interface was sufficient to operate the devices, and no external voltage bias was necessary to operate the detectors. Preliminary calculations on intrinsic detection efficiency indicate values between 1.6% and 2.6%.

I. Introduction

Semiconductor detectors coated with neutron reactive materials offer an alternative approach to scintillator-based neutron imaging devices for neutron radiography (normally scintillating screens coupled to photographic film or to other photorecording devices). Neutron reactive film-coated devices investigated in previous works include Si, bulk GaAs, and diamond detectors, all of which have advantages and disadvantages [1-5]. Si and bulk GaAs-based devices operate at moderately low voltages, whereas diamond-based films require hundreds of volts to operate. Although diamond-based films appear to be more radiation hard than GaAs, GaAs devices demonstrate superior radiation hardness to neutrons and gamma rays in comparison to Si. Neutron reactive films based on the ^{157}Gd(n,γ)^{158}Gd reaction show a higher neutron absorption efficiency than ^{10}B(n,α)^{7}Li and ^{6}Li(n,α)^{3}H-based films, however the combined emission of low energy gamma rays and conversion electrons from ^{157}Gd(n,γ)^{158}Gd reactions make neutron-induced events difficult to discriminate from background gamma-ray events. The particle energies emitted from the ^{6}Li(n,α)^{3}H reaction are greater than those emitted from the ^{10}B(n,α)^{7}Li reaction and are much greater than observed from the ^{157}Gd(n,γ)^{158}Gd reaction. Yet, the optimized film thickness for ^{6}LiF is over ten times greater than needed for ^{10}B while producing only a slight increase in neutron detection efficiency. Background gamma rays are less likely to interact in a diamond or Si detector than in GaAs, but previous results have shown that the gamma-ray background interference for ^{10}B-coated GaAs detectors is low enough to discriminate between neutron and gamma-ray events. Hence, ^{10}B-coated GaAs detectors offer a good compromise for the desired detector properties.

II. Theoretical Considerations and Detector Design

A. ^{10}B Film Coatings and Expected Efficiency

The ^{10}B(n,α)^{7}Li reaction leads to the following reaction products and branching ratios [6]:

$$^{10}\mathrm{B} + \mathrm{n} \rightarrow \begin{cases} 6\%: & ^{7}\mathrm{Li}(1.015\,\mathrm{MeV}) + \alpha\ (1.777\,\mathrm{MeV}), \\ & Q = 2.792\ \mathrm{MeV}(\textit{to ground state}) \\ 94\%: & ^{7}\mathrm{Li}^{*}(840\,\mathrm{keV}) + \alpha\ (1.470\,\mathrm{MeV}), \\ & Q = 2.310\ \mathrm{MeV}(\textit{1st excited state}) \end{cases}$$

The thermal neutrons (0.0259 eV) absorbed by ^{10}B produce energetic particles that are at a 180° angle. After absorption, 94% of the reactions leave the ^{7}Li ion in its first excited state which rapidly de-excites to the ground state (~ 10^{-13} seconds) by releasing a 480 keV gamma ray. The remaining 6% of the reactions result in the ^{7}Li ion going directly to its ground state. The thermal neutron (0.0259 eV) microscopic absorption cross section is 3840 barns. The microscopic thermal neutron absorption cross section decreases with increasing neutron energy; thus the cross section dependence is proportional to the inverse of the neutron velocity ($1/v$)

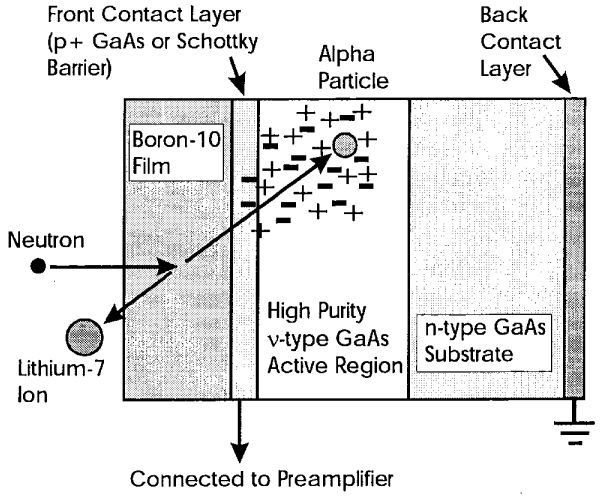

Fig. 1. The basic construction of a ^{10}B-coated self-biased high-purity epitaxial GaAs neutron detector. Neutrons interact in the ^{10}B film, thereby releasing an alpha particle and a ^{7}Li ion in opposite directions. Only one particle from the interaction can enter the detector. The built-in potential at the contact/ν-type GaAs interface supplies enough voltage to operate the device.

0018-9499/00$10.00

over much of the energy range [7,8].

In the following article, the term "effective range" (denoted L) is the distance through which a particle may travel *within the neutron reactive film* before its energy decreases below the set minimum detectable threshold, or rather, before its energy decreases below the electronic lower level discriminator (*LLD*) setting. The term does not take into account additional energy losses from contact "dead regions". The neutron reaction products released do not have equal masses, and therefore do not have equal energies or effective ranges. The short-range reaction product effective range is denoted L_{SR} and the long-range reaction product effective range is denoted L_{LR}.

Neutrons may interact anywhere within the reactive film, and the reaction products lose energy as they move through the neutron reactive film. Reaction product self-absorption reduces the energy transferred to the semiconductor detector, and ultimately limits the maximum film thickness that can be deposited over the semiconductor device. The measured voltage signal is directly proportional to the number of electron-hole pairs excited within the semiconductor. Reaction products that deposit most or all of their energy in the detector will produce much larger voltage signals than those reaction products that lose most of their energy before reaching the detector.

Neutron transmission through the film as a function of distance x can be described by

$$I(x) = I_0 e^{-x\sigma_F N_F} = I_0 e^{-x\Sigma_F} , \qquad (1)$$

where I_0 is the initial neutron flux, N_F is the atomic density of the neutron reactive isotope in the film, σ_F is the microscopic thermal neutron absorption cross section of the film, and Σ_F is the film macroscopic thermal neutron absorption cross section. The fraction of neutrons absorbed in the film through distance x is

$$1 - \frac{I(x)}{I_0} = 1 - e^{-x\sigma_F N_F} = 1 - e^{-x\Sigma_F} . \qquad (2)$$

The neutron absorption probability per unit distance is described by

$$P(x)dx = \Sigma_F e^{-x\Sigma_F} dx . \qquad (3)$$

The angular contribution to self-attenuation must also be addressed. Once a neutron is absorbed and the reaction products are emitted, the probability that a reaction product particle will enter the detector is determined by the solid angle that the particle effective range allows [4]. A neutron interaction taking place at distance x from the detector has a probability of entering the detector as described by the fractional solid angle that subtends the detector,

$$P_p(x) = \frac{\Omega(x)}{4\pi} = \frac{2\pi}{4\pi}\left(1 - \frac{x}{L}\right) = 0.5\left(1 - \frac{x}{L}\right), x \le L \quad (4)$$

where the subscript p relates to the reaction product particle of interest. Since the reactions of interest in the present work release two different charged-particle reaction products per event, the total probability of detecting a reaction necessitates adding the detection probabilities of both particles. It is completely possible that one reaction product may be able to reach the detector while the other reaction product can not [4]. Interactions occurring near the detector contact result in either particle entering the detector with high probability. As the neutron interaction distance increases, the solid angle of the short-range particle decreases more rapidly than that of the long-range particle, which results in an overall decrease in detection sensitivity.

As mentioned previously, the primary $^{10}B(n,\alpha)^7Li$ reaction (94%) results in the emission of a 1.47 MeV alpha particle and a 840 keV ^7Li ion in its first excited state. For the remaining $^{10}B(n,\alpha)^7Li$ reactions, the ^7Li ion reduces directly to its ground state resulting in the emission of a 1.777 MeV alpha particle and a 1.015 MeV ^7Li ion. The average range for a 840 keV ^7Li ion in boron is 1.6 microns, and the average range for a 1.47 MeV alpha particle is 3.6 microns.

The energy absorbed in the detector is simply the original particle energy minus the combined energy lost in the boron film and the detector contact during transit. Assuming that energy loss in the detector contact is negligible, Figure 2 shows the energy retained by either charged particle as a function of transit length through the boron film. At any reaction location within the ^{10}B film, maximum detector entrance energy will be retained by either particle should either enter the detector in an orthogonal trajectory. Hence, if the interaction occurs in the ^{10}B film at a distance of 0.5 μm away from the detector, the maximum energy retained by the ^7Li ion will be 430 keV, and the maximum energy retained by the alpha particle will be 1150 keV. For the same interaction distance of 0.5 μm from the detector, the energy retained by the particle when it reaches the detector decreases as the angle increases from orthogonal.

Given a predetermined minimum detection threshold (or

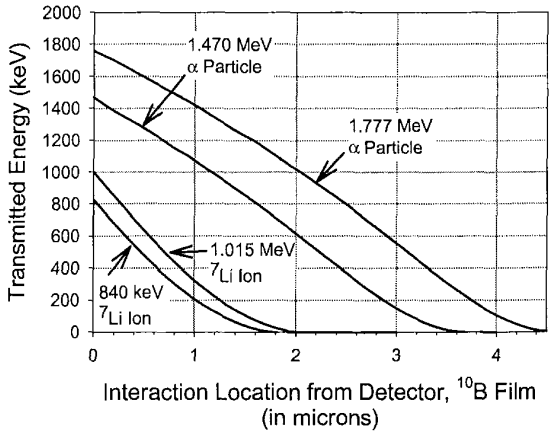

Fig. 2. Remaining energy of transmitted reaction products from the $^{10}B(n,\alpha)^7Li$ reaction as a function of interaction depth in the ^{10}B material *from* the contact interface. Contact attenuation was not considered. The calculation was performed for an orthogonal entrance angle.

LLD setting), the effective range (L) for either particle can be determined. For instance, from Figure 2, an *LLD* setting of 300 keV yields L_{Li} as 0.810 microns and L_α as 2.648 microns. With a microscopic thermal neutron absorption cross section (σ) for ^{10}B of 3840 barns and an atomic density of 1.3×10^{23} atoms/cm^3, the resulting macroscopic absorption cross section (Σ) is 500/cm.

A commonly used geometry involves the use of a planar semiconductor detector over which a neutron reactive film has been deposited. Assuming that the neutron beam is perpendicular to the detector front contact, the sensitivity contribution for a reaction product species can be found by integrating the product of the interaction probability (equation 3) and the fractional solid angle (equation 4) over the absorber ^{10}B film thickness (D_F) [4]:

$$S_p(D_F) = 0.5F_p\left\{\left(1+\frac{1}{\Sigma_F L}\right)\left(1-e^{-\Sigma_F D_F}\right)-\frac{D_F}{L}\right\} \quad , \quad (5A)$$

for $D \leq L$, and

$$S_p(D_F) = 0.5\,F_p\,e^{-\Sigma_F (D_F - L)}\left\{\left(1+\frac{1}{\Sigma_F L}\right)\left(1-e^{-\Sigma_F L}\right)-1\right\} \quad , \quad (5B)$$

for $D_F > L$, where F_p refers to the branching ratio of the reaction product emissions. The total sensitivity accordingly can be found by adding all of the reaction product sensitivities

$$S(D_F)\big|_{Total} = \sum_{p=1}^{N} S_p(D_F) \quad , \quad (6)$$

where N is the number of different reaction product emissions. In the case of ^{10}B-based films, N equals 4. Notice from equation 5*B* that the value of S_p reduces as D_F becomes larger than the value of L. As a result of this, there will be an optimum neutron reactive film thickness for front-irradiated detectors (see Figure 3). Since the minimum particle detection threshold determines the effective range (L), the optimum film thickness is also a function of the *LLD* setting.

B. GaAs Diode Structures

Two basic diode structures were investigated, both of which incorporated high-purity undoped GaAs epitaxial layers grown onto *n*-type GaAs substrates. The undoped GaAs regions had background impurity concentrations of $n = 3\text{x}10^{14}$/cm^3, yielding ν-type unintentionally-doped GaAs material. Two blocking contact adaptations were applied to the high-purity ν-type GaAs regions: 2000 Å thick $p+$ GaAs blocking contacts and 200 Å thick Schottky blocking contacts. Six variations of these structures were fabricated (see Table 1). The $p+$ contact and high-purity ν-type epitaxial GaAs films were grown by low-pressure metalorganic chemical vapor deposition. The ν-type GaAs active layers ranged between 1 micron and 5 microns in thickness. The device sensitive areas were 3mm x 3mm, each coated with a 1.5mm diameter film of 98% enriched high-purity ^{10}B. Two variations were coated with 6500 Å of ^{10}B, one with 7200 Å of ^{10}B, and three with 5000 Å of ^{10}B. The

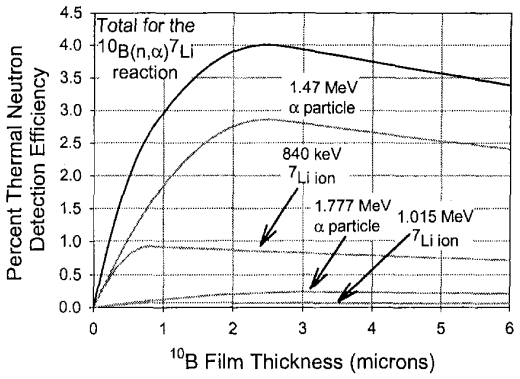

Fig. 3. Calculated detection efficiency for a ^{10}B-coated semiconductor detector. Energy attenuation in the contact region was not included. Shown are the contributions from the four charged-particle emissions and the total cumulative thermal neutron detection efficiency. *LLD* = 300 keV for the calculations.

detector elements were bonded to common T0-5 headers and tested for thermal neutron sensitivity in custom designed, light impenetrable aluminum boxes. The difference between the work functions of the blocking contacts ($p+$ GaAs layers or Schottky contacts) and the ν-type high-purity GaAs layers produces an internal potential difference at the film interface [9]. The "built-in" potential produces an internal electric field. The internal electric field is strong enough to deplete a good portion of the ν-type GaAs region and transport a considerable fraction of the charge carriers excited by the charged particle across the active ν-type region. Therefore, external voltage bias is not required to operate the devices. Voltage need only be applied in order to operate the supporting readout electronics. The basic *p-n* junction approximation [9] indicates that the built-in potential should deplete at least 1.5 microns of the ν-type region. The Schottky barrier devices demonstrated slightly higher reverse leakage currents than the $p+$ contact devices, an expected result due to the lower barrier height generally formed by Schottky contacts as compared to *p-i-n* structures. Furthermore, the built-in potential of the *p-i-n* structure is higher than the Schottky barrier structure due to the larger difference in work functions between the $p+$ region and the ν-type GaAs region, resulting in a higher internal electric field.

Energy self-absorption from ions crossing the 2000 Å $p+$ layer will ultimately reduce the amount of energy deposited directly in the detector. Assuming that electron-hole pairs excited in the $p+$ region do *not* contribute to the measured output signal, calculations indicate that energy lost from 840 keV ^7Li ions crossing the $p+$ region will range between 40 and 100 keV depending upon the particle trajectory and $^{10}B(n,\alpha)^7Li$ reaction location [10]. Additionally, the average energy lost from 1.47 MeV alpha particles crossing the $p+$ region will be 74 keV. Yet, such a view is somewhat pessimistic in that a significant portion of excited electrons can diffuse from the $p+$ region into the ν-type region whereupon they will be collected and contribute to the output signal. Regardless, the thin 200 Å Schottky barriers should have much less charge loss in the contact region than the $p+$

Table 1: High-Purity GaAs Diodes Investigated as Neutron Detectors

Sample Number	Diode Type	Boron-10 Thickness	Blocking Contact	ν-type GaAs ($n = 3x10^{14}/cm^3$)	Intermediate Layer	Substrate
3241	*p-i-n*	5000 Å	*p*+ GaAs ($2x10^{19}/cm^3$) 2000 Å	5 μm thick	None	*n*-type GaAs
3242	*p-i-n*	6500 Å	*p*+ GaAs ($2x10^{19}/cm^3$) 2000 Å	2 μm thick	None	*n*-type GaAs
3243	*p-i-n*	7200 Å	*p*+ GaAs ($2x10^{19}/cm^3$) 2000 Å	5 μm thick	None	*n*-type GaAs
3246	*p-i-n*	5000 Å	*p*+ GaAs ($2x10^{19}/cm^3$) 2000 Å	1 μm thick	None	*n*-type GaAs
3247	*p-i-n*	5000 Å	*p*+ GaAs ($2x10^{19}/cm^3$) 2000 Å	2 μm thick	*n*-type $Al_XGa_{1-X}As$ ($5x10^{15}/cm^3$) 2500 Å	*n*-type GaAs
3278	Schottky Diode	6500 Å	Au Schottky Contact 200 Å	5 μm thick	None	*n*-type GaAs

contact devices, so that a direct comparison can be made between the two styles of devices.

III. Experimental Arrangement and Results

Various detectors from all six diode configurations were tested in a beam port from a thermal neutron reactor (Ford Nuclear Reactor at the University of Michigan). The neutron beam was doubly diffracted through copper plates and collimated through a combined Benelex beam stop and polyethylene block. All detectors were tested under zero bias conditions. The devices were installed into aluminum testing boxes designed to reduce radiofrequency (RF) and photoelectric noise. The boxes were also designed with cylindrical, close-ended, hollow chimneys on them, enabling repeatable indexing of the detector into the same location of the thermal neutron beam. Each detector was mounted such that it fit into the hollow chimney. Afterwards, the chimney was inserted into a polyethylene collar that fit snugly into the receiving end of a beam port polyethylene-collimated block. The detector was connected through the aluminum box to an Ortec 142A preamplifier. The signals were shaped in an amplifier and recorded on a multichannel analyzer. One-hour duration measurements were performed. Dead time was adjusted such that it was maintained at 2%.

Figures 5 through 10 show representative spectra from the various GaAs diode samples. Although all devices worked, certain unique characteristics can be understood from the various spectra. A reaction product spectrum from sample diode 3241A is shown in Figure 5; the four major charged particle reaction products of the $^{10}B(n,\alpha)^7Li$ reaction are clearly apparent. Some energy self-absorption occurs in the thin 5000 Å ^{10}B film. The 5 μm thick ν-type GaAs layer is thick enough to absorb the full energy of the higher energy alpha-particle emissions. The device "built-in" potential is high enough to deplete the *n*-type GaAs region such that most or all of the energy from the reaction products can be absorbed. It is also apparent that the spectrum is constituted primarily from charged-particle reaction products and not background gamma rays. The device is not designed to be a spectrometer for charged-particle reaction products, but instead a simple low-powered neutron counter. However, the reaction product spectrum clearly shows that the device is (a) detecting neutron reaction product species and (b) has a sufficiently high gamma-ray-to-neutron-rejection ratio.

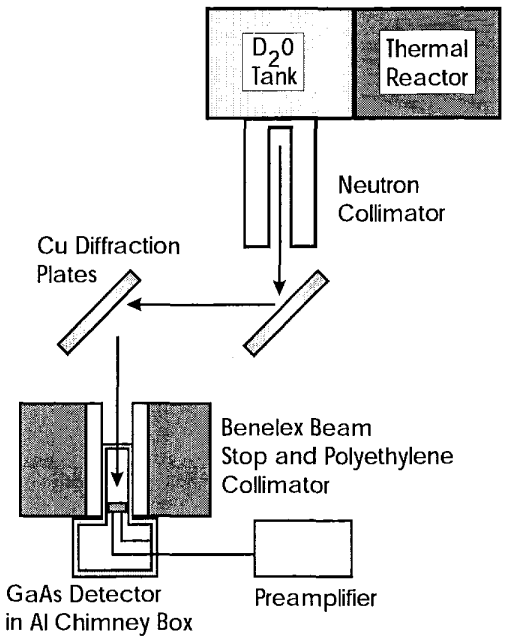

Fig. 4. Experimental configuration for thermal neutron detection with the self-biased ^{10}B-coated GaAs devices. The aluminum chimney ensured consistent alignment within the neutron beam.

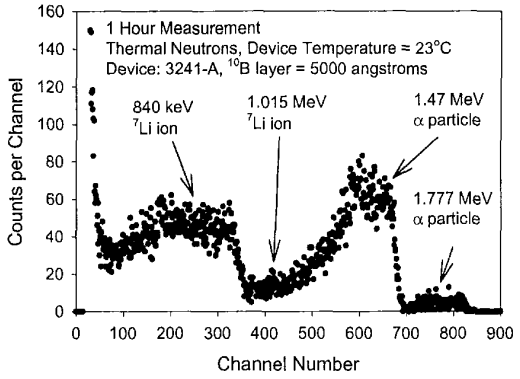

Fig. 5. Pulse height spectrum from sample diode 3241A of thermal neutron reactions in ^{10}B. All of the major charged-particle reaction product energies are apparent. No voltage was applied to the device during the measurement.

Sample diode 3241C was reverse biased up to 31 volts before breaking down, but only a slight difference in the pulse height spectrum was observed, within which the maximum channel number for the 1.777 MeV ^{7}Li ion increased from approximately 830 to 850. The minor improvement in performance indicates that ν-type region was fully active in charge collection from the built-in potential. Average neutron detection efficiency was 1.6%.

Figure 6 shows a spectrum from sample diode 3242A, a device similar to sample 3241A, but with only a 2 μm thick ν-type GaAs layer. Sample 3242A also has 6500 Å of deposited ^{10}B rather than 5000 Å. None of the reaction product energies are discernable, indicating that the active region of the device is not absorbing the full energies of the charged particles. Average neutron detection efficiency was 2.3%.

Figure 7 shows a spectrum from sample diode 3243A, and although the diode construction was similar to 3241A, 7200 Å of ^{10}B was deposited over it. The negative slope in the

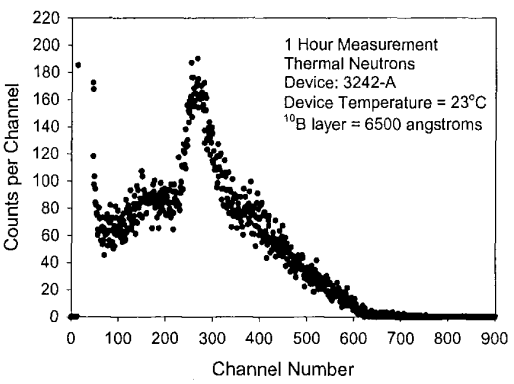

Fig. 6. Pulse height spectrum from sample diode 3242A of thermal neutron reactions in ^{10}B. None of the major charged-particle reaction product energies are discernable. No voltage was applied to the device during the measurement. The artifact peak appears as a result of incomplete energy deposition in the device active region.

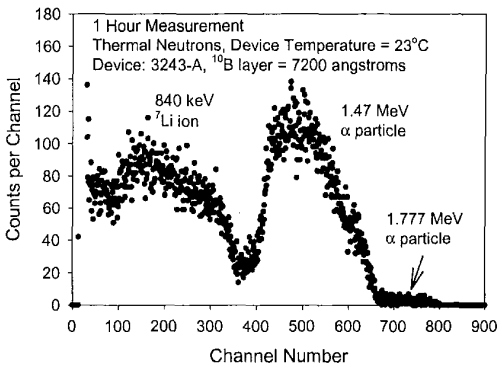

Fig. 7. Pulse height spectrum from sample diode 3243A of thermal neutron reactions in ^{10}B. All of the major charged-particle reaction product energies are apparent. No voltage was applied to the device during the measurement.

device energy spectrum is indicative of energy self absorption, in which the combined effect of the $p+$ layer and the ^{10}B film have reduced and dispersed the pulse height spectrum to a greater extent than detectors from sample 3241. Some improvement is observed when the diode is reverse biased, yet the distinctive shape remains. Average neutron detection efficiency was 2.62%, comparing well to the expected value from Figure 3.

Figure 8 shows a spectrum from sample diode 3246A. Within a very thin ν-type active region (only 1μm), the spectrum shows artifact peaks, although not quite as distincly as the diodes from sample 3242. The clear separation of the 840 keV ^{7}Li peak is expected with the thin ^{10}B layer. Surprisingly, the maximum energy deposition is not very much less than seen for samples 3241 and 3243, denoting that much of the charge excited external to the active region is being recorded. Hence, a considerable fraction of charge carriers are diffusing from both the $p+$ contact layer and the n-type substrate layer into the active region. Average neutron

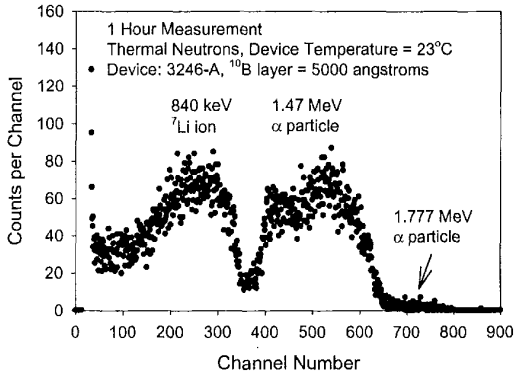

Fig. 8. Pulse height spectrum from sample diode 3246A of thermal neutron reactions in ^{10}B. All of the major charged-particle reaction product energies are apparent. No voltage was applied to the device during the measurement. The satellite artifact peak appears as a result of incomplete energy deposition in the device active region.

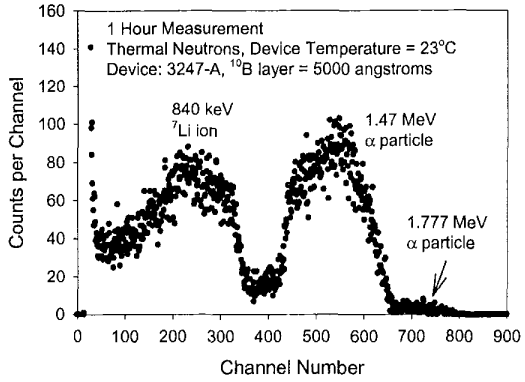

Fig. 9. Pulse height spectrum from sample diode 3247A of thermal neutron reactions in ^{10}B. All of the major charged-particle reaction product energies are apparent. No voltage was applied to the device during the measurement.

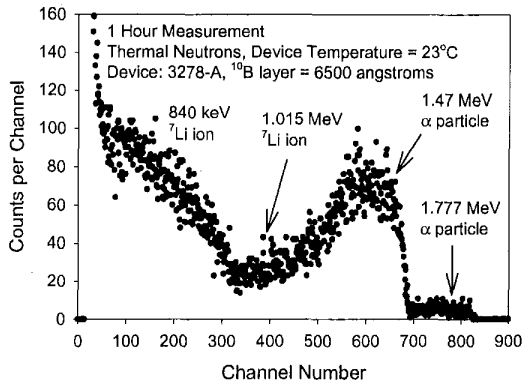

Fig. 10. Pulse height spectrum from sample diode 3278A of thermal neutron reactions in ^{10}B. All of the major charged-particle reaction product energies are apparent. No voltage was applied to the device during the measurement. More energy is retained due to the thin Schottky contact, but the device clearly has higher electronic noise.

detection efficiency was 1.7%.

Figure 9 shows a spectrum from sample diode 3247A. The diode has a similar construction to sample 3242, except that a 2500 Å thick *n*-type $Al_XGa_{1-X}As$ layer was grown betweenthe ν-type active region and the *n*-type substrate. The *n*-type $Al_XGa_{1-X}As$ layer was added in an attempt to confine electron-hole pairs to the active region of the detector by means a of a small bandgap step. Here we see that the performance was not very different than 3243A. The dispersion of the 1.47 MeV alpha-particle peak is most likely a compound effect from both energy self-absorption in the ^{10}B layer and *p*+ contact layer and also energy loss from transmission of particles into the *n*-type substrate. Again, the clear observation of the major charged-particle energy peaks indicates that diffusing charges from the *p*+ region and the *n*-type $Al_XGa_{1-X}As$ layer are participating in charge collection. Average neutron detection efficiency was 1.9%, comparing well to the expected value shown in Figure 3.

Figure 10 shows a spectrum from sample diode 3278A,which is a Schottky barrier device. All devices from sample 3278 were electronically noisier than the *p*+ contact devices. Additionally, the devices did not withstand any appreciable reverse-bias voltage before breaking down. The absence of the 2000 Å *p*+ layer reduces energy self-absorption, which is apparent since the only other devices with energy resolution showing all four reaction product energies are from sample 3241 (sample 3241 had the same thickness of active region as samples from 3278 with the ^{10}B layer reduced by 1500 Å). In other words, the combined total thickness of the contact and converter layer were very similar, with only a difference of approximately 500 Å between sample 3241 and 3278. Average neutron detection efficiency was 2.2% for 3278.

IV. Conclusions

Self-biased devices from all six samples demonstrated counting efficiency similar to the expected efficiency, indicating that the ν-type regions need not be very thick to operate as viable, low-power neutron counters. The best spectral performance was observed from sample 3241, and the best counting efficiency from sample 3243. The worst spectral performance was from sample 3242, although the counting efficiency matched almost exactly to theoretical values. The Schottky barrier devices (3278) did perform well, although they demonstrated higher electronic noise and could not hold any appreciable reverse voltage.

The self-biased design offers a straightforward method to produce low-cost, lightweight, compact and low-power neutron detectors for remote deployment. Future devices will have thicker ^{10}B films to increase neutron detection efficiency closer to the theoretical maximum indicated in Figure 3. Stacking the devices can further increase thermal neutron detection efficiency. Various detectors from the six samples are presently being irradiated with fast and thermal neutrons as well as gamma rays in order to determine their radiation hardness and the limiting radiation doses through which the different configurations may survive.

V. References

[1] A. Rose, "Sputtered Boron Films on Silicon Surface Barrier Detectors," Nucl. Instr. and Meth., 52, pp. 166-170, 1967.

[2] B. Feigl and H. Rauch, "Der Gd-Neutronenzähler," Nucl. Instr. and Meth., 61, pp. 349-356, 1968.

[3] A. Mireshghi, G. Cho, J.S. Drewery, W.S. Hong, T. Jing, H. Lee, S.N. Kaplan and V. Perez-Mendez, "High Efficiency Neutron Sensitive Amorphous Silicon Pixel Detectors," IEEE Trans. Nucl. Sci., NS-41, pp. 915-921, 1994.

[4] D.S. McGregor, J.T. Lindsay, C.C. Brannon and R.W. Olsen, "Semi-insulating Bulk GaAs Thermal Neutron Imaging Arrays," IEEE Trans. Nucl. Sci., NS-43, pp.1357-1364, 1996.

[5] F. Foulon, P. Bergonzo, A. Brambilla, C. Jany, B. Guizard and R.D. Marshall, "Neutron Detectors Made from Chemically Vapour Deposited Semiconductors," Proc. MRS, 487, pp.591-

596, 1998.
[6] G.F. Knoll, Radiation Detection and Measurement, 2nd Ed. (Wiley, New York, 1989).
[7] D.I. Garber and R.R. Kinsey, BNL 325: Neutron Cross Sections, 3rd Ed., Vol. 2, Curves (Brookhaven National Laboratory, Upton, 1976).
[8] V. McLane, C.L. Dunford and P.F. Rose, Neutron Cross Sections, Vol. 2 (Academic Press, San Diego, 1988).
[9] S.M. Sze, Physics of Semiconductor Devices, 2nd Ed. (Wiley, New York, 1981).
[10] J.F. Ziegler and J.P. Biersack, SRIM-2000 Code, Version 9 (IBM Company, 1998).